Frontiers in Bioscience Landmark

Front. Biosci. (Landmark Ed) **2026**; 31(4): 52067
https://doi.org/10.31083/FBL52067

Original Research

Context-Dependent Modulation of Macrophage Plasticity by Cordycepin Drives Tumor Regression in Melanoma

Jihae Lim[1,†], Donglan Piao[1,†], Jio Kang[1], Suh Jin Yoon[1,2], Hyun Ji Lee[1,2], Isoo Youn[1], Eun Kyoung Seo[1,*], Eun Sook Hwang[1,2,*]

[1]College of Pharmacy and Graduate School of Pharmaceutical Sciences, Ewha Womans University, 03760 Seoul, Republic of Korea
[2]Graduate Program in Innovative Biomaterials Convergence, Ewha Womans University, 03760 Seoul, Republic of Korea
*Correspondence: yuny@ewha.ac.kr (Eun Kyoung Seo); eshwang@ewha.ac.kr (Eun Sook Hwang)
[†]These authors contributed equally.
Academic Editor: Graham Pawelec
Submitted: 4 December 2025 Revised: 19 March 2026 Accepted: 3 April 2026 Published: 27 April 2026

Abstract

Background and Aim: Cordycepin (CDC), an adenosine (ADO) analog from *Cordyceps* mushrooms, exhibits potent anti-tumor and immunomodulatory activities. However, the precise mechanisms governing its effects on macrophage plasticity remain poorly understood. This study aimed to isolate CDC from a high-yielding *Cordyceps* cultivar, validate its systemic anti-tumor efficacy, and elucidate the mechanobiological cues regulating CDC-driven macrophage functions under varying cell-density states. **Experimental Procedure**: CDC (>98% purity) was isolated and structurally characterized via nuclear magnetic resonance (NMR) and high-resolution electrospray ionization mass spectrometry (HR-ESI-MS). Primary bone marrow-derived macrophages and RAW264.7 cells, cultured under sparse (~30%) or confluent (100%) conditions, were treated with CDC or ADO. We evaluated cell viability, pro-inflammatory cytokine expression, and Nuclear Factor kappa B (NF-κB) p65 signaling, phagocytosis, and migration. The therapeutic potential of CDC-primed macrophages was assessed via *in vitro* melanoma co-culture and *in vivo* intratumoral adoptive transfer in B16F10 tumor-bearing mice. **Key Results**: Systemic administration of CDC significantly inhibited melanoma growth *in vivo*, promoting apoptosis, enhancing macrophage infiltration. We discovered that CDC regulates macrophage functions via a density-dependent "switch": while CDC induced cytotoxicity in sparse cultures, it significantly augmented M1-like cytokine production in confluent states without compromising viability. This density-dependent activation was mediated by the A2A adenosine receptor (A2AR), triggering the Akt–NF-κB p65 signaling axis. Furthermore, CDC upregulated migration- and phagocytosis-associated genes, enhancing tumor cell clearance. Notably, intratumoral injection of CDC-primed macrophages markedly reduced tumor volume and size *in vivo*. **Conclusions and Implications**: CDC modulates macrophage activation through a unique mechanobiological switch. Under high-density conditions—mimicking the dense tumor microenvironment—CDC enhances A2AR-mediated NF-κB activation, boosting macrophage activation, recruitment, and phagocytosis to facilitate tumor regression. These findings establish CDC as a context-dependent immunomodulator capable of reprogramming macrophages toward a tumoricidal phenotype.

Keywords: cordycepin; tumor microenvironment; A2A adenosine receptor; macrophage plasticity; mechanobiology

1. Introduction

Cordycepin (CDC), a bioactive nucleoside analog from *Cordyceps* spp., is widely recognized for its potent anti-diabetic, anti-tumor, and anti-metastatic activities [1–3]. Structurally analogous to adenosine (ADO) but lacking a 3′-hydroxy group, CDC enters cells via nucleoside transporters [4] to disrupt RNA and DNA synthesis, thereby inhibiting tumor cell proliferation and inducing apoptosis [4,5]. Beyond direct cytotoxicity, CDC modulates immune responses by interacting with extracellular ADO receptors (A2AR, A2BR, and A3R), which significantly influences tumor progression [6–10].

Recent paradigms in precision medicine emphasize the role of natural bioactive compounds in fine-tuning immune signaling pathways, particularly the MAPK and NF-κB axes, to modulate inflammatory landscapes [11]. Within this framework, macrophages serve as central targets for therapeutic intervention due to their remarkable functional plasticity and their emerging role as innovative vehicles for targeted cancer treatments [12–15]. CDC is extensively documented for its anti-inflammatory effects, suppressing hyper-inflammatory responses in lipopolysaccharide (LPS)-induced macrophages by inhibiting Nuclear Factor kappa B (NF-κB) signaling and the Nucleotide-binding oligomerization domain (NOD)-like Receptor family Pyrin domain containing 3 (NLRP3) inflammasome [16–19]. Furthermore, CDC has been shown to promote M2-like macrophage polarization, which facilitates tissue repair and the resolution of inflammation [20,21].

However, a functional paradox exists regarding the role of CDC in the tumor microenvironment (TME). Effective tumor clearance often requires the robust activation of M1-like macrophages—characterized by the secretion of pro-inflammatory cytokines such as IL-1β, IL-6,

and TNFα—to overcome the immunosuppressive nature of the TME [22,23]. The existing literature primarily focuses on the CDC-induced M1-to-M2 shift, which does not fully account for its observed anti-tumor efficacy in contexts where M1 activation is advantageous. This discrepancy highlights a critical need to explore how CDC reconfigures macrophage functional plasticity under dynamic environmental cues, such as varying cell densities.

In this study, we investigated the potential of CDC, isolated from a novel *Cordyceps* cultivar, to reprogram macrophage plasticity depending on environmental physical cues. We aimed to elucidate by which CDC modulates macrophage functional states to enhance anti-tumor immunity, thereby providing a strategic rationale for its application as a targeted immunotherapeutic agent within the complex tumor microenvironment.

2. Materials and Methods

2.1 Materials

A standard reference of CDC was purchased from Sigma-Aldrich (St. Louis, MO, USA) for authentication. Recombinant cytokines were purchased from R&D Systems (Minneapolis, MN, USA). LPS, MG132, 4′,6-diamidino-2-phenylindole (DAPI), and ADO were sourced from Sigma-Aldrich or Cayman Chemical (Ann Arbor, MI, USA). Primary antibodies against pp65 (S536) (#3033), p65 (#8242), pIκB (S32) (#2859), Inhibitor of Nuclear Factor kappa B (IκB) (#4814), Akt (#4691), pAkt (S473) (#4060), IKKβ (#2684), p-p38 (T180/Y182) (#4511), pERK (T202/Y204) (#4370), and actin (#4970) were obtained from Cell Signaling Technology (Danvers, MA, USA). Antibodies for F4/80 (sc-377009) and CD68 (catalogue number sc-17832, lot number II) were from Santa Cruz Biotechnology, Inc. (Santa Cruz, CA, USA).

2.2 CDC Isolation and Characterization

CDC was isolated from *Cordyceps militaris* ARA301 (BIOARA Co., Ltd., Seoul, Korea), which was cultivated on a 100% edible insect medium. Briefly, 3 kg of *C. militaris* ARA301 was extracted using methanol. The crude extract was subsequently partitioned with *n*-hexane, ethyl acetate (EtOAc), and butanol (BuOH). The resulting fractions underwent silica gel and Diaion HP-20 chromatography. CDC was further purified through additional silica chromatography and crystallization, yielding 6.418 g of final product. The chemical structure of CDC was confirmed via $^{1}H/^{13}C$ nuclear magnetic resonance (NMR) and high-resolution electrospray ionization mass spectrometry (HR-ESI-MS) ($[M+H]^+$ *m/z* 252.1092, $C_{10}H_{13}N_5O_3$) [24]. Purity was validated to be >98% purity using high-performance liquid chromatography with ultraviolet detection (HPLC-UV) on a Hypersil GOLD C18 column (Thermo Scientific, Waltham, MA, USA, 0.5 mL/min flow rate, 30 °C, detection at 254 nm).

2.3 Cell Culture

Bone marrow (BM) cells were isolated from male C57BL/6 mice (8–10 weeks old, Orient Bio Inc., Gyeonggi-do, Korea) and plated at 2×10^6 cells/mL in 12-well plates. Primary bone marrow-derived macrophages (BMDMs) were characterized by the expression of lineage-specific markers (F4/80 and CD11b) via flow cytometry. The cells were cultured with macrophage colony-stimulating factor (M-CSF, 10 ng/mL, Sigma-Aldrich) for 6 days to generate mature macrophages. On day 6, confluent cells (representing high-density, contact-inhibited states) were treated with LPS (100 ng/mL), along with CDC and/or ADO for 24 h. In parallel, cells were re-plated at low-density (2×10^5 cells/mL) to stimulate a sparse environment and treated with LPS, CDC, and/or ADO for 24 h. Additionally, RAW264.7 (TIB-71) and B16F10 (CRL-6475) cells were purchased from the American Type Culture Collection (ATCC, Manassas, VA, USA). The authenticity of these cell lines was validated by Short Tandem Repeat profiling and they were confirmed to be negative for mycoplasma contamination before use. RAW264.7 cells were plated at 3×10^5 cells/mL (low-density) and 8×10^5 cells/mL (confluent) in 12-well plates, followed by treatment with CDC or ADO for 24 h in the presence of LPS (100 ng/mL).

2.4 Cell Viability/Cytotoxicity Assay

BM-derived M1 macrophages or RAW264.7 cells were treated with CDC or ADO for 24 h. Cells were subsequently incubated with EZ-Cytox reagent for 30 min, according to the manufacturer's instructions (EZ-Cytox Cell Viability Assay Kit, DoGenBio, Seoul, Korea). Cell viability was quantified by measuring optical density at 450 nm using a microplate reader (NFEC-2019-10-258101) (Molecular Devices, Sunnyvale, CA, USA) at the Ewha Fluorescence Imaging Core Center. Results were expressed relative to the vehicle-treated control.

2.5 Quantitative PCR (qPCR)

Total RNA was extracted using TRIzol reagent (Invitrogen, Carlsbad, CA, USA), and 2 µg of RNA were subjected to reverse transcription using MMLV Reverse Transcriptase (Promega, Madison, WI, USA). qPCR was performed using Thunderbird SYBR qPCR Mix (Toyobo, Osaka, Japan) on a StepOnePlus Real-Time PCR machine (Applied Biosystems, Carlsbad, CA, USA). Relative transcript levels were calculated using the comparative Ct ($2^{-\Delta\Delta Ct}$) method, with β-actin as the internal control. Primer sequences used were as follows: β-actin, 5′-agagggaaatcgtgcgtgac-3′ and 5′-tggatgccacaggattcc-3′; IL-6, 5′-gaggataccactcccaacaga-3′ and 5′-aagtgcatcatcgttgttcataca-3′; IL-1β, 5′-caaccaacaagtgatattctccat-3′ and 5′-gatccacactctccagctgca-3′; TNFα, 5′-cagttctatggcccagaccctca-3′ and 5′-acaacccatcggctggcaccac-3′; CD68, 5′-cctatacccaattcagggtgg-3′ and 5′-ctgcgccatgaatgtccac-

3′; monocyte chemoattractant protein 1 (MCP1), 5′-cttctgggcctgctgttca-3′ and 5′-ccagcctactcattgggatca-3′; and CC chemokine receptor 2 (CCR2), 5′-tggctgtgtttgcctctctaccag-3′ and 5′-caagtagaggcaggatcaggctc-3′.

2.6 Immunofluorescence and Immunoblot Analysis

Cells on poly-L-lysine-coated coverslips or culture slides (Marienfeld, Lauda-Königshofen, Germany) were treated with CDC, fixed, and stained with antibodies against NF-κB p65, followed by nuclear counterstaining with DAPI (1 µg/mL, Sigma-Aldrich). Fluorescence images were acquired using a fluorescence microscope (Axio Observer 7, Carl Zeiss, Oberkochen, Germany) (NFEC-2021-08-272462) at the Ewha Drug Development Research Core Center. For immunoblotting, cell lysates were prepared in RIPA buffer (50 mM Tris, pH 7.4, 150 mM NaCl, 1% NP-40, 0.5% sodium deoxycholate, and 0.1% sodium dodesyl sulfate), resolved by Sodium Dodesyl Sulfate-Polyacrylamide Gel Electrophoresis (SDS-PAGE), and transferred to membranes. Membranes were probed with primary and secondary antibodies, detected using an ImageQuant 800 (Cytiva, Marlborough, MA, USA), and quantified with ImageJ 1.53t software (NIH, Bethesda, MD, USA).

2.7 Reporter Gene Assay

RAW264.7 or HEK293T cells were transfected with NF-κB-luc or pIL-6-luc reporter constructs and RSVβ for normalization. Following 24-h treatment with CDC or ADO, luciferase and β-galactosidase activities were measured using the Luciferase Assay System kit (Promega, Madison, WI, USA) and the Galacto-Light Plus™ system (Applied Biosystems, Foster City, CA, USA), respectively. Luciferase activity was expressed as fold induction compared to control after normalization to β-galactosidase activity.

2.8 Phagocytosis and Migration Assays

For phagocytosis, cells were incubated fluorescence-conjugated zymosan bioparticles (ab234053, Abcam, Cambridge, MA, USA) at a final concentration of 5 µg/mL for 30 min at 37 °C. Phagocytic activity was analyzed via flow cytometry (FACS Calibur, BD Biosciences, San Jose, CA, USA). For the migration assay, treated M1 macrophages were placed in the upper chamber of a 24-well Transwell insert (5 µm pore size, MERCK Millipore, Billerica, MA, USA), with B16F10 melanoma cells in the lower chamber. After 5 h of incubation, cells on the upper surface of the membrane were removed, and migrated cells were stained with 0.2% crystal violet, imaged, and quantified.

2.9 In Vitro Tumor Killing

B16F10 melanoma tumor cells were labeled with carboxyfluorescein succinimidyl ester (CFSE, 5 µM) for 15 min. The CFSE-labeled tumor cells were co-cultured with macrophages pre-treated with CDC or ADO for 24 h. After co-culture, cells were stained with an anti-F4/80 antibody and analyzed by flow cytometry. Phagocytic macrophages and viable tumor cells were quantified using CellQuest software (BD Biosciences, San Jose, CA, USA).

2.10 In Vivo Anti-Tumor Study

Male C57BL6/J mice (10–12 weeks old) were anesthetized with isoflurane (3%) using a small-animal inhalation anesthetic system (3–5 min) and subcutaneously injected with B16F10 melanoma cells (5×10^5 cells/mouse). Mice were randomized into experimental groups. On day 10, after tumor establishment, macrophages pre-treated with CDC or vehicle were injected intratumorally (5×10^5 cells/mouse in 50 µL) under isoflurane anesthesia. Tumor growth was monitored for 14 days, after which the mice were euthanized for histological analysis.

2.11 Histology and Immunohistochemistry

Mice were euthanized by CO_2 inhalation (at a displacement rate of 20% of the chamber volume per minute to ensure ethical and humane sacrifice), and tumors were harvested, fixed in 10% formalin, and embedded in paraffin. Tumor sections (4 µm thick) were stained for F4/80 and CD68 with fluorescent secondary antibodies and DAPI (1 µg/mL, Sigma-Aldrich) for nuclear counterstaining. Apoptotic cell death was evaluated by terminal deoxynucleotidyl transferase dUTP nick-end labeling (TUNEL) staining, performed with a commercial kit (R&D Systems, 4810-30-K).

2.12 Statistical Analysis

Data are presented as the mean ± standard error of the mean (SEM) from at least five independent experiments. Statistical analysis was performed using GraphPad Prism version 10.0 (GraphPad Software LLC, San Diego, CA, USA). For comparisons between two groups, Student's *t*-test was employed. For comparisons involving three or more groups, one-way analysis of variance (ANOVA) followed by Tukey's post-hoc test was used. A significance level of $p < 0.05$ was used. For *in vivo* studies, investigators were blinded to the treatment groups during tumor measurement and histological analysis.

3. Results

3.1 CDC Exhibits Potent Anti-Tumor Activity and Increases Macrophage Infiltration

To obtain sufficient quantities of naturally occurring CDC, we utilized the high-yielding cultivar *C. militaris* ARA301. CDC was successfully isolated and purified from multiple fractions, yielding a total of 6.418 g from fractions XI-9 and BII (Fig. 1A). The identity and structural integrity of the purified compound were confirmed by $^{1}H/^{13}C$ NMR spectra, which were consistent with reported reference data [24]. High-resolution ESI-MS analysis con-

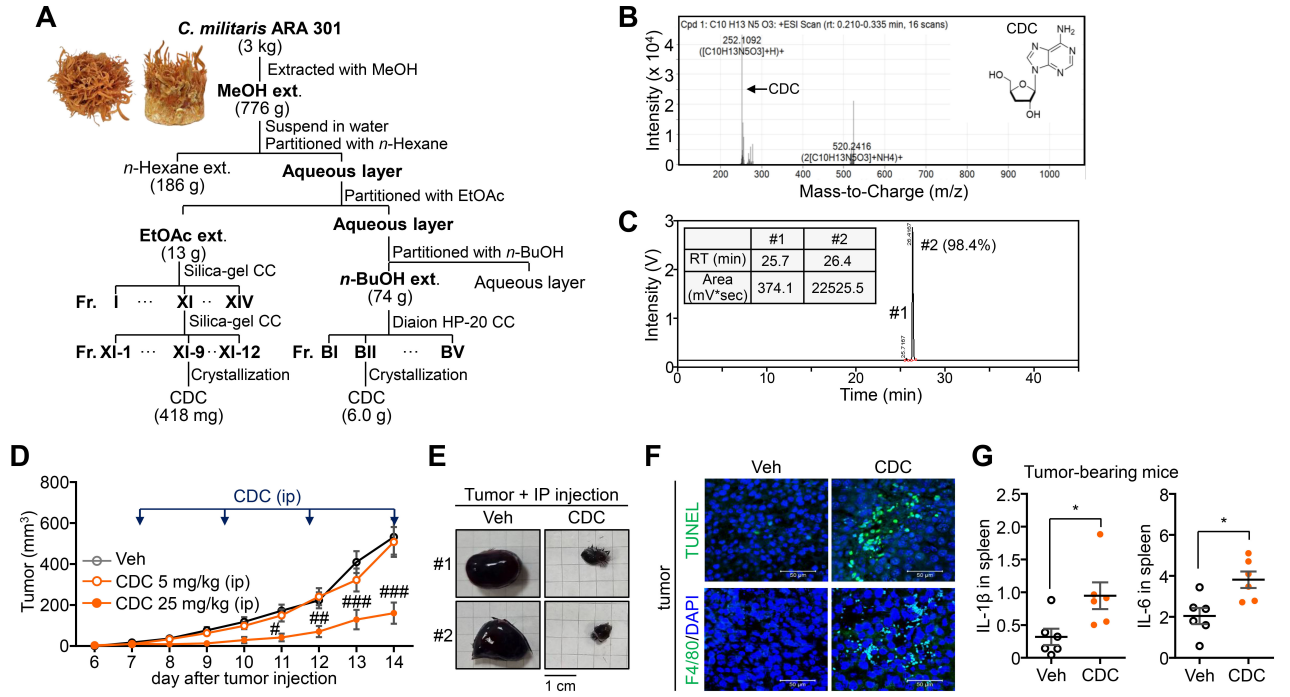

Fig. 1. Identification and anti-tumor activity of Cordycepin (CDC) isolated from a novel Cordyceps cultivar. (A) Isolation procedure and yield of CDC from *C. militaris* ARA301 cultivar. (B) High-resolution electrospray ionization mass spectrometry (HR-ESI-MS) analysis for the molecular weight determination of isolated CDC. (C) High-performance liquid chromatography with ultraviolet detection (HPLC-UV) chromatogram confirming the purity and identity of the CDC fraction. (D) Inhibitory effect of CDC on *in vivo* B16F10 melanoma tumor growth in a syngeneic mouse model. (E) Comparison of representative tumor sizes and weights at the study endpoint. Scale bar = 1 cm. (F) Histological analysis of tumor sections via terminal deoxynucleotidyl transferase dUTP nick-end labeling (TUNEL) staining (apoptosis) and F4/80 immunohistochemistry (macrophage infiltration). Scale bar = 50 µm. (G) qPCR analysis of IL-1β and IL-6 in the spleens of tumor bearing mice. Data are presented as mean ± standard error of the mean (SEM). Statistical significance: #$p < 0.05$; ##$p < 0.005$; ###$p < 0.0005$ as determined by one-way analysis of variance (ANOVA); *$p < 0.05$ by Student's *t*-test.

firmed the molecular formula as $C_{10}H_{13}N_5O_3$ (Fig. 1B). HPLC-UV analysis further verified a purity greater than 98% (Fig. 1C). To validate the *in vivo* anti-tumor efficacy of CDC, we administered the compound intraperitoneally to a melanoma mouse model. CDC treatment resulted in a significant inhibition of tumor growth, as evidenced by reduced tumor volume and size (Fig. 1D,E). Histological analysis of tumor tissues from CDC-treated mice revealed a marked increase in apoptotic cell death (TUNEL positive) and macrophage infiltration (F4/80 positive) (Fig. 1F). Furthermore, elevated systemic levels of pro-inflammatory cytokines were detected in the spleens of these mice, indicating a robust immune response (Fig. 1G). Collectively, these findings suggest that CDC not only inhibits tumor progression but also significantly enhances macrophage activation and recruitment within the TME, contributing to its overall anti-tumor effects.

3.2 CDC Exhibits Cell Density-Dependent Cytotoxicity in Macrophages via Mechanical Microenvironmental Cues

Given prior reports indicating that CDC can reduce cell viability [16,17,25], we first evaluated its cytotoxic effects on BM-derived M1 macrophages across a range of concentrations. In confluent (100% density) cultures, CDC exhibited no significant cytotoxicity at concentrations up to 20 µM, with viability decreasing only at concentrations above 50 µM (Fig. 2A). As macrophage activation and functional states are known to be modulated by physical cues and mechanical forces [26–28], we examined whether cell density affects CDC's efficacy. Notably, while CDC remained non-cytotoxic in confluent M1 macrophages, it significantly reduced cell numbers in low-density (approx. 30%) cultures at concentrations of 10–20 µM (Fig. 2B). A consistent pattern was observed in RAW264.7 macrophages, where CDC-induced cytotoxicity was strictly confined to low-density conditions (Fig. 2C). In contrast, the structural analog ADO resulted in no significant loss of viability in either M1 or RAW264.7 macrophages, regardless of cell density (Fig. 2D,E). These findings demonstrate that CDC-induced cytotoxicity is uniquely contingent upon cell density, suggesting that mechanically-driven changes in the microenvironment—such as altered cell-to-cell contact or cytoskeletal tension—fundamentally reconfigure the macrophage response to CDC.

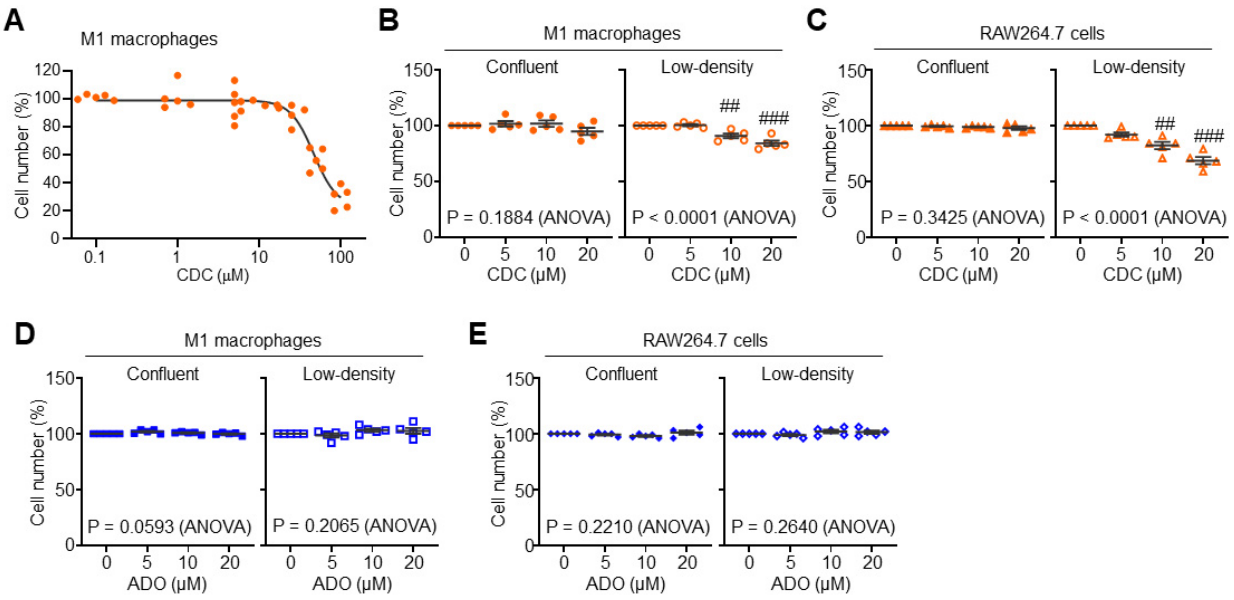

Fig. 2. Context-dependent modulation of macrophage viability by CDC and adenosine (ADO). (A) Dose-dependent effects of CDC on the viability of BM-derived M1 macrophages across a range of concentrations (0.1~100 μM). (B) Modulation of M1 macrophage viability by CDC under varying cell densities (confluent vs. low-density). (C) Cell viability modulation of RAW264.7 cells treated with CDC in confluent and low-density cultures. (D) Effects of ADO on M1 macrophage viability in confluent and low-density conditions. (E) Cell viability modulation of RAW264.7 cells following ADO treatment under confluent and low-density conditions. Data are presented as mean ± SEM. Statistical significance: ##$p < 0.005$; ###$p < 0.0005$ as determined by one-way ANOVA.

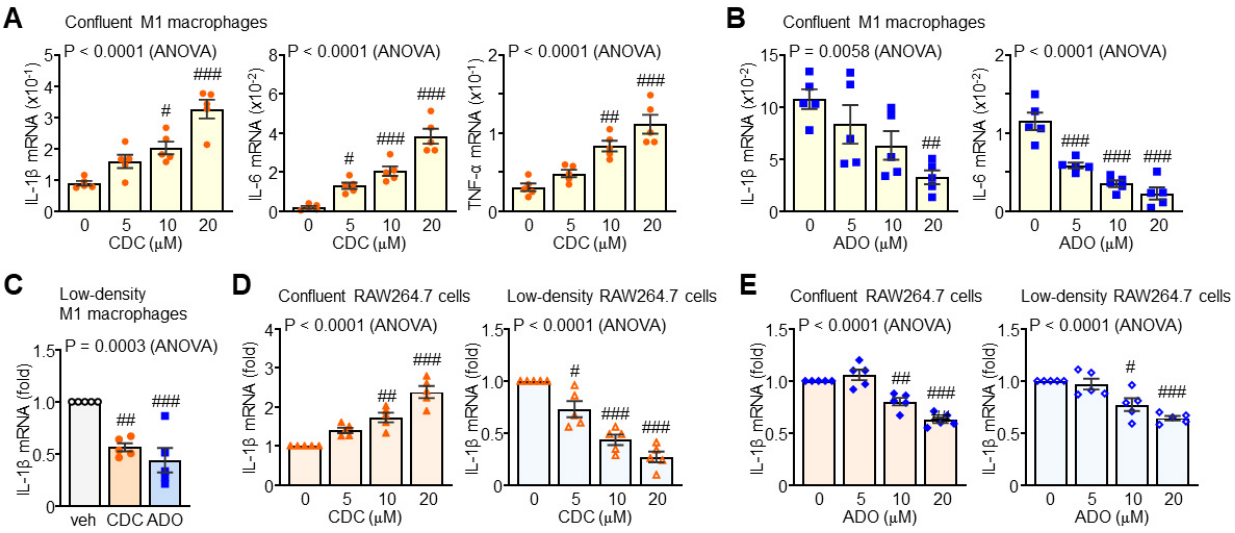

Fig. 3. Context-dependent modulation of inflammatory cytokine transcripts by CDC and ADO. (A) Regulatory effects of CDC on pro-inflammatory cytokine mRNA expression in confluent M1 macrophages. (B) Inhibitory effects of ADO on pro-inflammatory cytokine expression in confluent M1 macrophages. (C) Comparative modulation of cytokine profiles by CDC or ADO in low-density M1 macrophages. (D) Density-dependent effects of CDC on pro-inflammatory cytokine expression in RAW264.7 cells (confluent vs. low-density). (E) Suppression of pro-inflammatory cytokines by ADO in RAW264.7 cells across varying culture densities. Statistical significance: #$p < 0.05$; ##$p < 0.005$; ###$p < 0.0005$ as determined by one-way ANOVA.

3.3 CDC Exerts Context-Dependent Modulation of Pro-Inflammatory Cytokine Production Based on Cell Density

We next measured inflammatory cytokine expression in both confluent and low-density cultures of BM-derived M1 macrophages and RAW264.7 cells. In confluent M1 macrophages, treatment with non-cytotoxic concentrations of CDC (≤20 μM) significantly enhanced the expression of IL-1β, IL-6, and TNFα, whereas ADO substantially suppressed their expression under the same con-

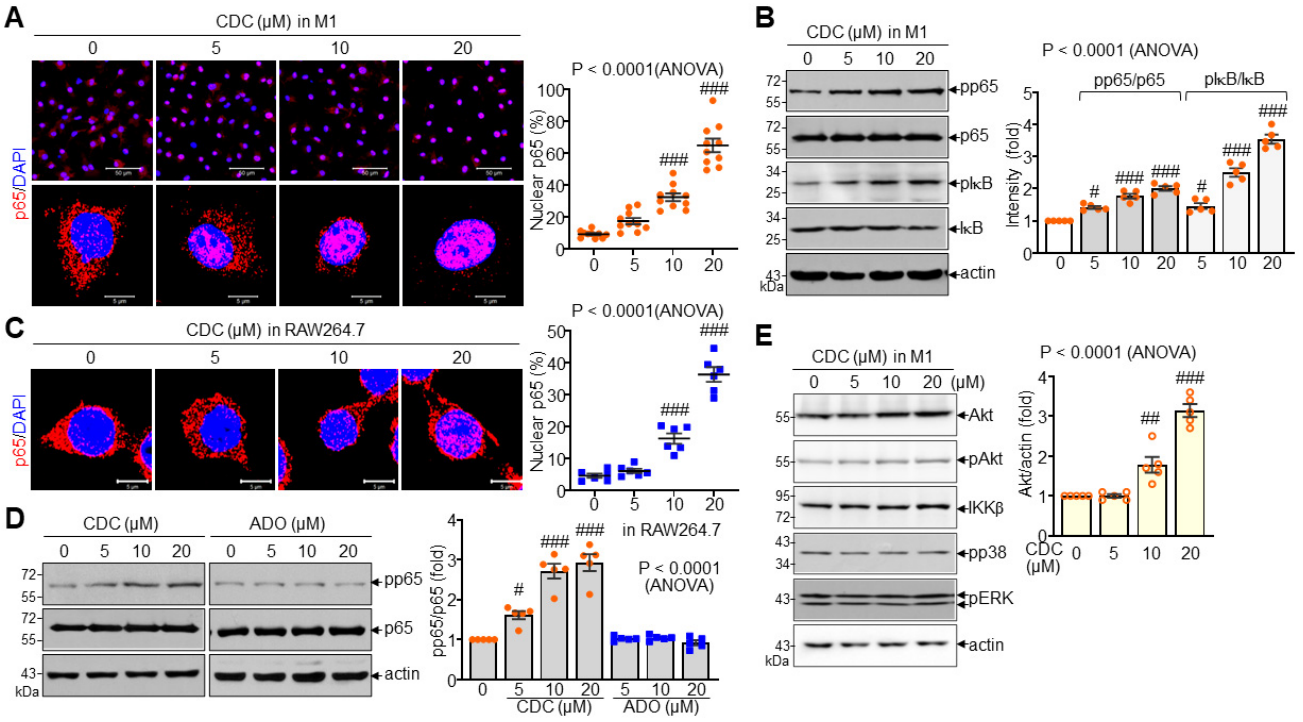

Fig. 4. Enhancement of p65 nuclear localization and phosphorylation by CDC. (A) Representative immunofluorescence images and quantitative analysis of p65 nuclear localization in M1 macrophages following CDC treatment. Scale bar = 50 μm (top) and 5 μm (bottom). (B) Immunoblot analysis and densitometric quantification of phosphorylated p65 (pp65), total p65, pIκB, and total Inhibitor of Nuclear Factor kappa B (IκB). Actin was used as a loading control. (C) Immunofluorescence staining and intensity quantification of p65 in RAW264.7 cells. Scale bar = 5 μm. (D) Protein expression levels of p-p65 and total p65 in RAW264.7 cells treated with CDC or ADO, including quantification of the p-p65/p65 ratio. (E) Immunoblot analysis of upstream signaling mediators of the Nuclear Factor kappa B (NF-κB) pathway in M1 macrophages, with corresponding densitometric quantification of total Akt. Statistical significance: #$p < 0.05$; ##$p < 0.005$; ###$p < 0.0005$ as determined by one-way ANOVA.

ditions (Fig. 3A,B). However, a starkly different pattern emerged under low-density culture conditions; CDC suppressed the expression of IL-1β, an effect associated with the concomitant density reduction in cell viability. Notably, while ADO also suppressed IL-1β expression in low-density conditions, it did so without altering cell viability (Fig. 3C). This density-dependent shift was consistently observed in RAW264.7 cells; CDC significantly increased pro-inflammatory cytokine production in confluent cultures but suppressed it in low-density cultures where cell viability was compromised (Fig. 3D). Unlike CDC, ADO persistently reduced cytokine production regardless of cell density or its effect on cell number (Fig. 3E). Collectively, these data demonstrate that CDC's immunomodulatory effects are fundamentally governed by the cellular microenvironment.

3.4 CDC Enhances NF-κB p65 Activation via Akt Upregulation in Macrophages

To elucidate the molecular mechanisms by which CDC induces immunomodulatory cytokine production, we examined the activation of the NF-κB pathway. Immunofluorescence analysis revealed that CDC dose-dependently increased the nuclear translocation of p65 in M1 macrophages (Fig. 4A). Furthermore, immunoblot analysis demonstrated that CDC enhanced the phosphorylation of p65 (pp65) and IκB without altering the total protein levels of p65 or IκB (Fig. 4B). Similar increases in p65 nuclear localization and phosphorylation were observed in CDC-treated RAW264.7 cells (Fig. 4C,D), whereas ADO exhibited no significant effect on p65 phosphorylation, distinguishing CDC's unique signaling profile (Fig. 4D). Further mechanistic analysis revealed that CDC significantly increased the total Akt expression—a key upstream regulator of the NF-κB axis—without affecting IκB kinase (IKK) levels or the activation of p38 and ERK MAPKs (Fig. 4E). This expansion of the total Akt pool likely facilitates the subsequent phosphorylation and nuclear localization of p65. Collectively, our findings suggest that the functional activation of macrophages by CDC is primarily driven by this Akt-dependent enhancement of the NF-κB signaling axis, providing a molecular basis for its pro-inflammatory and anti-tumor effects.

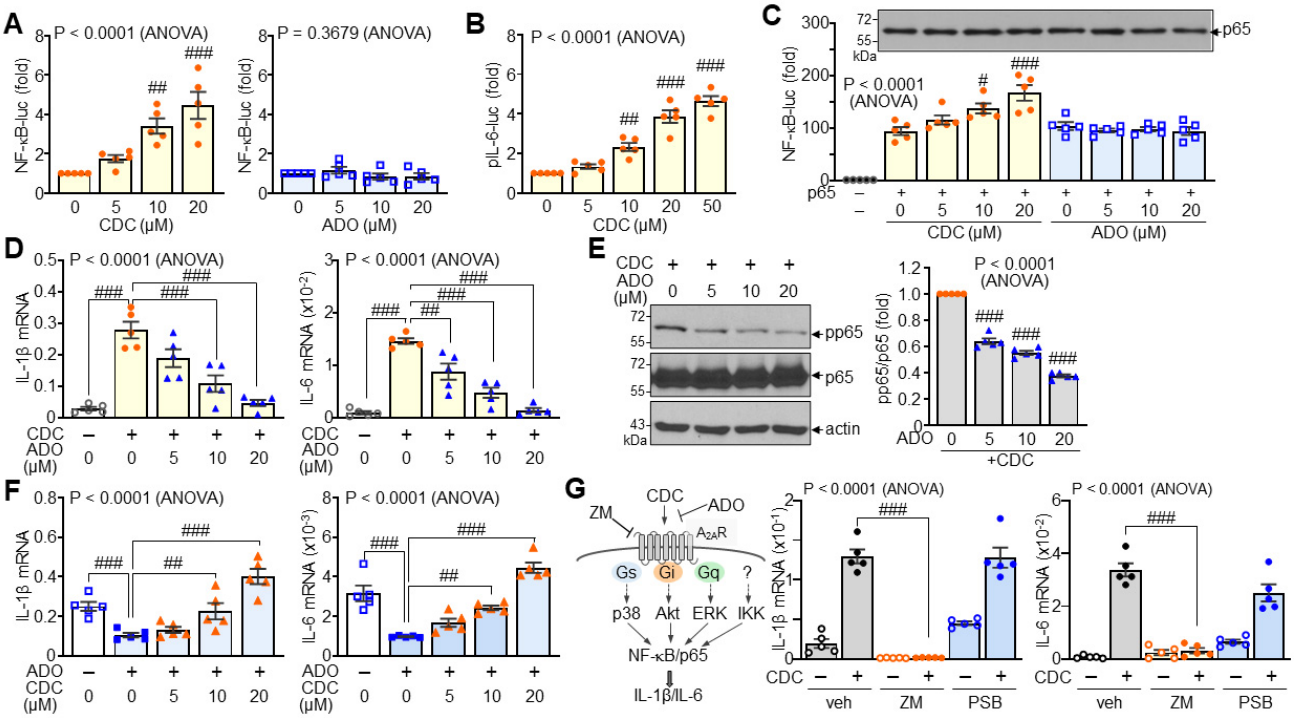

Fig. 5. Activation of A2A adenosine receptor (A2AR)-mediated signaling by CDC. (A) Reporter assay measuring NF-κB-luc activity in RAW264.7 cells following treatment with CDC or ADO. (B) pIL-6-luc reporter activity in RAW264.7 cells treated with CDC. (C) NF-κB-luc reporter activity in p65-transfected HEK-293T cells treated with CDC or ADO (bar graph). Immunoblot analysis confirming the uniform expression of transfected p65 protein across groups. (D) qPCR analysis for IL-1β and IL-6 in M1 macrophages treated with ADO (5~20 μM) in the presence of CDC (10 μM). (E) Immunoblot analysis and densitometric quantification of pp65 and total p65 in M1 macrophages. (F) qPCR analysis of IL-1β and IL-6 in M1 macrophages treated with CDC (5~20 μM) in the presence of ADO (10 μM). (G) Schematic illustration of the proposed A2AR-mediated signaling, alongside qPCR analysis of IL-1β and IL-6 following treatment with CDC and/or the A2AR-selective antagonist ZM241385 (ZM, 10 μM) or the A2BR-selective antagonist PSB-603 (PSB, 10 μM). Statistical significance: #$p < 0.05$; ##$p < 0.005$; ###$p < 0.0005$ as determined by one-way ANOVA.

3.5 CDC Engages A2AR-Mediated Signaling in Competition With ADO

Consistent with its effect on NF-κB p65 phosphorylation, CDC, not ADO, significantly increased NFκB and IL6 promoter reporter activities in RAW264.7 cells in a dose-dependent manner (Fig. 5A,B). Furthermore, the elevated NF-κB-luc activity induced by p65 overexpression in HEK293T cells was dose-dependently enhanced by CDC, whereas ADO showed no significant effect (Fig. 5C). These contrasting pharmacological profiles prompted us to investigate whether CDC competes with ADO for A2AR-mediated signaling. We observed that ADO inhibited CDC-induced production of IL-6 and IL-1β in a dose-dependent manner (Fig. 5D) and markedly reduced CDC-induced phosphorylation of p65 (Fig. 5E). Conversely, CDC restored inflammatory cytokine production that had been suppressed by ADO (Fig. 5F), suggesting a competitive interaction between the two nucleoside analogs at the receptor level. To definitively identify the ADO receptor subtype involved, cells were treated with selective antagonists. Notably, the A2AR-specific antagonist ZM241385 significantly attenuated CDC-induced increases in IL-6 and IL-1β. In contrast, the A2BR-selective antagonist (PSB-603) exerted no inhibitory effect under the same conditions (Fig. 5G), confirming that the immunostimulatory effects of CDC are specifically mediated through A2AR. Collectively, these findings demonstrate that CDC engages A2AR signaling in competition with ADO, thereby promoting the Akt-dependent NF-κB axis and enhancing the production of immunomodulatory cytokines.

3.6 CDC Enhances Macrophage Phagocytosis and Migration

Building on the engagement of A2AR–Akt–NF-κB signaling, we assessed the functional impact of CDC on macrophage phagocytic activity and migration. Phagocytosis assays using zymosan bioparticles demonstrated that CDC significantly increased phagocytic capacity of both M1 and RAW264.7 macrophages, whereas ADO showed no significant effect (Fig. 6A). This functional enhancement was markedly suppressed by the A2AR antagonist ZM241385, confirming that CDC stimulates phagocytosis specifically through A2AR pathway (Fig. 6B). In addi-

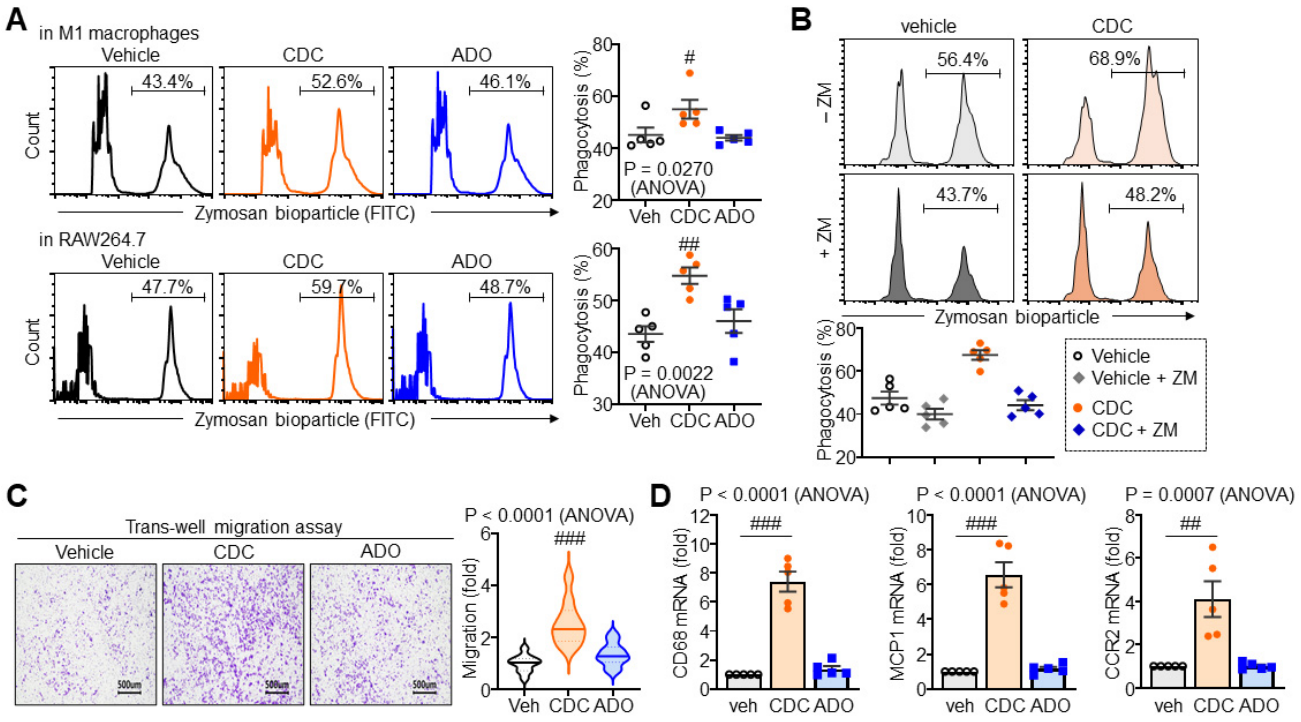

Fig. 6. Enhancement of macrophage phagocytosis and migratory capacity by CDC. (A) Representative images and quantitative analysis of phagocytic activity in M1 macrophages and RAW264.7 cells following treatment with CDC (20 µM) or ADO (20 µM). (B) Phagocytosis assay and corresponding quantification of M1 macrophages in the presence or absence of the A2AR antagonist ZM241385 (ZM, 10 µM). (C) Transwell migration assay and quantification of M1 macrophages following treatment with 20 µM CDC or ADO. Scale bar = 500 µm. (D) qPCR analysis of migration-related markers (CD68, monocyte chemoattractant protein 1 (MCP-1), and CC chemokine receptor 2 (CCR2)) in M1 macrophages treated with CDC. Statistical significance: #$p < 0.05$; ##$p < 0.005$; ###$p < 0.0005$ as determined by one-way ANOVA.

tion to phagocytosis, we evaluated macrophage migration, a critical factor for tumor infiltration. CDC significantly promoted macrophage chemotaxis toward B16F10 melanoma cells, while ADO exhibited no effect on the migratory capacity of RAW264.7 cells (Fig. 6C). Consistent with this increased motility, CDC, but not ADO, upregulated the expression of key migration- and recruitment-associated genes, including CD68, MCP1, and CCR2 (Fig. 6D). These results indicate that CDC promotes a comprehensive anti-tumor phenotype by enhancing both macrophage phagocytosis and migration. These effects, mediated by A2AR signaling, likely facilitate the recruitment of activated macrophages to the tumor site and their subsequent clearance of malignant cells, distinguishing CDC from its endogenous analog, ADO.

3.7 CDC Suppresses Tumor Growth via Macrophage Activation In Vitro and In Vivo

Having established that CDC enhances macrophage migration and phagocytosis, we evaluated its anti-tumor effects in co-culture and syngeneic mouse models. CFSE-labelled B16F10 melanoma cells were co-cultured with M1 macrophages pre-treated with either CDC or ADO. CDC-treated M1 macrophages exhibited a significantly increased phagocytic uptake of tumor cells but ADO did not (Fig. 7A). Consequently, tumor cell viability was markedly reduced in co-cultures with CDC-pre-treated M1 macrophages, and this tumoricidal effect was further enhanced when macrophages were primed with CDC. However, ADO treatment failed to produce any significant enhancement in tumor killing (Fig. 7B,C). To assess *in vivo* efficacy, mice bearing subcutaneous melanomas received intratumoral injections of either vehicle-treated or CDC-treated M1 macrophages. CDC-activated M1 macrophages significantly suppressed tumor growth, resulting in a substantial reduction in both tumor volume and weight compared to vehicle-treated macrophage controls (Fig. 7D,E). Histological analysis of the tumor tissues confirmed the therapeutic mechanism: tumors receiving CDC-primed macrophages showed a marked increase in apoptotic cell death (TUNEL positive) and a higher density of CD68-positive macrophage infiltration (Fig. 7F). These findings demonstrate that CDC functionally re-programs M1 macrophages into a potent tumoricidal phenotype, enhancing their ability to infiltrate the tumor mass and execute tumor cell clearance, thereby suppressing tumor progression *in vivo*.

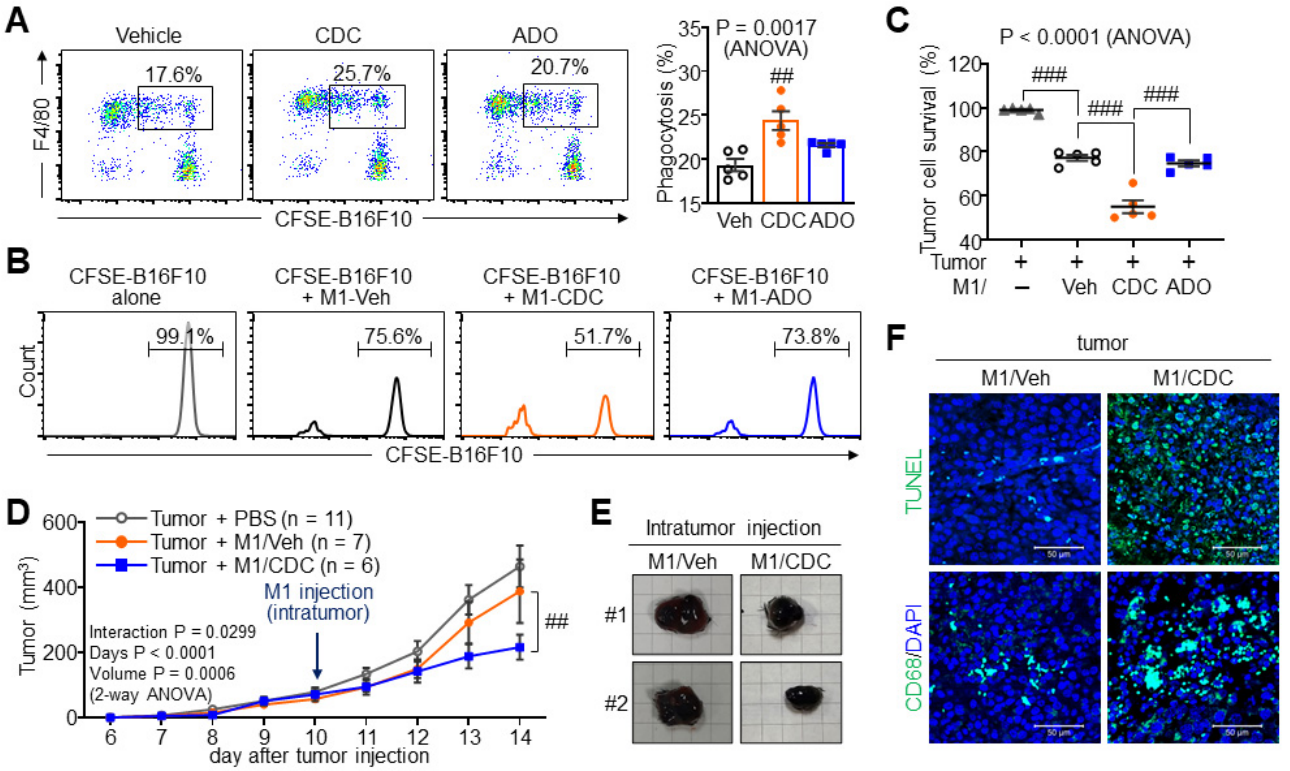

Fig. 7. Anti-tumor efficacy of CDC-activated M1 macrophages. (A) Tumor phagocytosis assay of M1 macrophages treated with 20 μM CDC or ADO co-cultured with carboxyfluorescein succinimidyl ester (CFSE)-labeled B16F10 melanoma cells. (B,C) Tumor cell survival assay in the presence of M1 macrophages. Survival of live B16F10 cells was analyzed by flow cytometry (B) and corresponding quantification (C). (D–F) Therapeutic evaluation in a syngeneic B16F10 tumor model (C57BL/6 mice) following intratumoral injection of vehicle- or CDC-pre-treated M1 macrophages. (D) Longitudinal tumor growth curves over the experimental period. (E) Comparison of terminal tumor size and mass. Each grid square is 0.5 cm. (F) Representative images of TUNEL staining (apoptosis) and CD68 staining (macrophage infiltration) in tumor sections. Sacle bar = 50 μm. Statistical significance: ##$p < 0.005$; ###$p < 0.0005$ as determined by one-way ANOVA.

4. Discussion

Our study demonstrates that CDC activates M1 macrophages and enhances anti-tumor functions by engaging the A2AR–Akt–NF-κB signaling axis. This engagement leads to the increased production of immunomodulatory cytokines, enhanced macrophage migration, and improved phagocytic activity, thereby facilitating tumor cell clearance *in vitro* and suppressing tumor progression *in vivo*.

While CDC is often recognized for its anti-inflammatory effects, our findings highlight its broader, more nuanced role in modulating macrophage plasticity within the TME. Although pro-inflammatory cytokines such as IL-1β and IL-6 can play complex roles in chronic inflammation, their acute induction is essential for "breaking" tumor immune tolerance and recruiting cytotoxic T lymphocytes and natural killer cells. In this context, CDC acts as a targeted immunotherapeutic rheostat, restoring the immunogenic potential of the TME by shifting immunosuppressive states toward a tumoricidal M1-like phenotype.

CDC, a nucleoside analog structurally similar to ADO, exerts its effects through AR-dependent signaling. Our comparative analysis with ADO and the use of the AR-selective antagonists confirms that CDC's pro-inflammatory effects are specifically mediated through the A2AR axis. Because CDC and ADO share structural motifs and compete for similar receptor populations, their functional relationship is intrinsically linked. However, CDC possesses a unique, density-dependent "switch" that is absent in standard ADO signaling, allowing it to bypass the typical immunosuppressive cues of the TME.

Previous studies indicated that CDC suppresses NF-κB p65 activation and IL-1β production in RAW264.7 cells at concentrations $\geq$20 μM [16–18]. In contrast, our findings reveal that CDC induces p65 activation and IL-1β production in confluent and high-density environments. This discrepancy likely underscores the decisive role of the physical microenvironment, where cell-to-cell contact and mechanical sensing [26,27] serve as fundamental determinants of CDC's efficacy. We propose that contact inhibition in confluent environments induces metabolic quiescence,

which reduces the metabolic turnover of CDC by adenosine kinase. This allows CDC to remain available for a longer duration as a potent signaling ligand for membrane-bound A2AR, triggering the Akt-NF-κB axis instead of being sequestered for intracellular metabolism.

Notably, CDC-induced functional reprogramming extends beyond phagocytosis to a significantly enhanced migratory capacity. We confirmed that CDC upregulates not only CD68 and MCP-1 but also CCR2, effectively priming macrophages for active tumor infiltration. This density-dependent transition—from a cytotoxic agent in sparse conditions to a potent immunostimulator in confluent states—provides a novel mechanobiological insight into how CDC reconfigures the inflammatory landscape based on the physical architecture of the tumor.

Mechanistically, CDC was found to enhance total Akt expression, providing a larger signaling reservoir for p65 phosphorylation. While ADO remained functionally inert regarding migration and recruitment markers, CDC's ability to integrate mechanical cues allows it to overcome the restrictive conditions that typically favor M2 exhaustion. In conclusion, CDC promotes macrophage activation and anti-tumor activity associated with enhanced migration and phagocytosis, driven by a unique sensitivity to the cellular microenvironment. This study establishes CDC as a promising candidate for reprogramming the TME, warranting further clinical characterization of its context-dependent therapeutic applications.

5. Limitations

Despite the significant findings of this study, several limitations should be acknowledged. First, while we demonstrated the density-dependent "switch" of CDC *in vitro* using primary BMDMs and RAW264.7 cells, the precise mechanical sensors (such as Piezo1 or integrin-mediated signaling) that interact with the A2AR-Akt axis remain to be fully identified. Second, although the B16F10 melanoma model provided a robust platform for validating systemic and adoptive transfer efficacy, further validation in diverse syngeneic or orthotopic tumor models is required to generalize the immunomodulatory role of CDC across different tumor architectures. Lastly, the long-term systemic effects of CDC-primed macrophage therapy on other organ systems were not extensively evaluated in this study, which may impact the clinical translation of this approach regarding potential off-target inflammatory responses.

6. Conclusions

In conclusion, this study demonstrates that Cordycepin (CDC) functions as a context-dependent immunomodulator that reconfigures macrophage plasticity through a mechanobiological switch. Unlike its endogenous analog adenosine, CDC promotes an M1-like tumoricidal phenotype specifically under high-density conditions—characteristic of the dense tumor microenvironment—by activating the A2AR–Akt–NF-κB signaling axis. These findings provide a strategic rationale for using CDC not only as a direct anti-tumor agent but also as a potent tool for macrophage-based immunotherapy, offering a novel approach to overcoming the immunosuppressive nature of solid tumors.

Abbreviations

ADO, Adenosine; ANOVA, Analysis of Variance; AR, Adenosine receptor; BM, Bone Marrow; BMDMs, Bone Marrow-Derived Macrophages; CCR2, CC chemokine receptor 2; CDC, Cordycepin; CFSE, Carboxyfluorescein succinimidyl ester; DAPI, 4′,6-Diamidino-2-Phenylindole; HPLC, High-Performance Liquid Chromatography; HR-ESI-MS, High-Resolution Electrospray Ionization Mass Spectrometry; IACUC, Institutional Animal Care and Use Committee; IκB, Inhibitor of Nuclear Factor kappa B; IKK, Inhibitor of nuclear factor kappa B kinase; LPS, Lipopolysaccharide; MCP1, monocyte chemoattractant protein 1; M-CSF, Macrophage Colony-Stimulating Factor; NF-κB, Nuclear Factor kappa B; PBS, Phosphate-buffered saline; SEM, Standard error of the mean; TME, Tumor microenvironment; TUNEL, Terminal deoxynucleotidyl transferase dUTP nick-end labeling.

Availability of Data and Materials

The datasets used and/or analyzed during the current study are available from the corresponding author on reasonable request.

Author Contributions

JL: Formal Analysis, Investigation, Methodology, Visualization, Writing – Original Draft Preparation. DP: Investigation, Methodology, Resources. JK: Formal Analysis, Investigation, Methodology, Visualization. SJY: Investigation, Validation, Data Curation. HJL: Investigation, Methodology, Validation. IY: Methodology, Software, Writing – Original Draft Preparation. EKS: Conceptualization, Resources, Supervision, Writing – Reviewing and Editing. ESH: Conceptualization, Funding Acquisition, Supervision, Visualization, Writing – Original Draft Preparation, Writing – Reviewing and Editing. All authors contributed to editorial changes in the manuscript. All authors read and approved the final manuscript. All authors have participated sufficiently in the work and agreed to be accountable for all aspects of the work.

Ethics Approval and Consent to Participate

All animal experiments were conducted in strict compliance with the NIH Guide for the Care and Use of Laboratory Animals and the national guidelines provided by the Ministry of Food and Drug Safety of Korea. The study protocols were formally reviewed and approved by the Institu-

tional Animal Care and Use Committee (IACUC) of Ewha Womans University (Approval Nos. IACUC 19-031 and IACUC 24-046). All efforts were made to minimize animal suffering during the experimental procedures. Animal experiments should adhere to the 3Rs principle: substitution, reduction, and optimization.

Acknowledgment

Not applicable.

Funding

This work was supported by the National Research Foundation of Korea [RS-2025-00558072 and RS-2021-NF000578], funded by the Ministry of Science and ICT.

Conflicts of Interest

The authors declare no conflicts of interest. Given the role as the Guest Editor and Editorial Board member, the corresponding author Eun Sook Hwang had no involvement in the peer-review of this article and has no access to information regarding its peer review. Full responsibility for the editorial process for this article was delegated to Graham Pawelec.

Declaration of AI and AI-Assisted Technologies in the Writing Process

During the preparation of this work, the author(s) used Gemini (Google) to refine the manuscript's English language and to assist in creating the graphical abstract. The author(s) reviewed and edited the AI-generated output and take(s) full responsibility for the final content.

References

[1] Khan MA, Tania M. Cordycepin in Anticancer Research: Molecular Mechanism of Therapeutic Effects. Current Medicinal Chemistry. 2020; 27: 983–996. https://doi.org/10.2174/0929867325666181001105749.

[2] Kim KM, Kwon YG, Chung HT, Yun YG, Pae HO, Han JA, *et al*. Methanol extract of Cordyceps pruinosa inhibits in vitro and in vivo inflammatory mediators by suppressing NF-kappaB activation. Toxicology and Applied Pharmacology. 2003; 190: 1–8. https://doi.org/10.1016/s0041-008x(03)00152-2.

[3] Sun H, Zhang A, Gong Y, Sun W, Yan B, Lei S, *et al*. Improving effect of cordycepin on insulin synthesis and secretion in normal and oxidative-damaged INS-1 cells. European Journal of Pharmacology. 2022; 920: 174843. https://doi.org/10.1016/j.ejphar.2022.174843.

[4] Yoon SY, Lindroth AM, Kwon S, Park SJ, Park YJ. Adenosine derivatives from Cordyceps exert antitumor effects against ovarian cancer cells through ENT1-mediated transport, induction of AMPK signaling, and consequent autophagic cell death. Biomedicine & Pharmacotherapy. 2022; 153: 113491. https://doi.org/10.1016/j.biopha.2022.113491.

[5] Chou SM, Lai WJ, Hong TW, Lai JY, Tsai SH, Chen YH, *et al*. Synergistic property of cordycepin in cultivated Cordyceps militaris-mediated apoptosis in human leukemia cells. Phytomedicine: International Journal of Phytotherapy and Phytopharmacology. 2014; 21: 1516–1524. https://doi.org/10.1016/j.phymed.2014.07.014.

[6] Cao HL, Liu ZJ, Chang Z. Cordycepin induces apoptosis in human bladder cancer cells via activation of A3 adenosine receptors. Tumour Biology: the Journal of the International Society for Oncodevelopmental Biology and Medicine. 2017; 39: 1010428317706915. https://doi.org/10.1177/1010428317706915.

[7] Chen Y, Yang SH, Hueng DY, Syu JP, Liao CC, Wu YC. Cordycepin induces apoptosis of C6 glioma cells through the adenosine 2A receptor-p53-caspase-7-PARP pathway. Chemico-biological Interactions. 2014; 216: 17–25. https://doi.org/10.1016/j.cbi.2014.03.010.

[8] Kim J, Shin JY, Choi YH, Lee SY, Jin MH, Kim CD, *et al*. Adenosine and Cordycepin Accelerate Tissue Remodeling Process through Adenosine Receptor Mediated Wnt/β-Catenin Pathway Stimulation by Regulating GSK3b Activity. International Journal of Molecular Sciences. 2021; 22: 5571. https://doi.org/10.3390/ijms22115571.

[9] Nakamura K, Shinozuka K, Yoshikawa N. Anticancer and antimetastatic effects of cordycepin, an active component of Cordyceps sinensis. Journal of Pharmacological Sciences. 2015; 127: 53–56. https://doi.org/10.1016/j.jphs.2014.09.001.

[10] Nakamura K, Yoshikawa N, Yamaguchi Y, Kagota S, Shinozuka K, Kunitomo M. Antitumor effect of cordycepin (3'-deoxyadenosine) on mouse melanoma and lung carcinoma cells involves adenosine A3 receptor stimulation. Anticancer Research. 2006; 26: 43–47.

[11] Wang P, Huang X, Geng S, Huang G, Pi W, Han N, *et al*. Herb-based multicomponent carrier-free hydrogel with antipyretic and anti-inflammatory dual effects by regulating MAPK and NF-κB signaling pathway. Materials Today. Bio. 2025; 35: 102371. https://doi.org/10.1016/j.mtbio.2025.102371.

[12] Atri C, Guerfali FZ, Laouini D. Role of Human Macrophage Polarization in Inflammation during Infectious Diseases. International Journal of Molecular Sciences. 2018; 19: 1801. https://doi.org/10.3390/ijms19061801.

[13] Rodríguez-Morales P, Franklin RA. Macrophage phenotypes and functions: resolving inflammation and restoring homeostasis. Trends in Immunology. 2023; 44: 986–998. https://doi.org/10.1016/j.it.2023.10.004.

[14] Yunna C, Mengru H, Lei W, Weidong C. Macrophage M1/M2 polarization. European Journal of Pharmacology. 2020; 877: 173090. https://doi.org/10.1016/j.ejphar.2020.173090.

[15] Ji M, Liu H, Liang X, Wei M, Shi D, Gou J, *et al*. Harnessing macrophages for precision drug delivery and cancer therapy: Strategies, advances and challenges. Materials Today. Bio. 2025; 35: 102535. https://doi.org/10.1016/j.mtbio.2025.102535.

[16] Kim HG, Shrestha B, Lim SY, Yoon DH, Chang WC, Shin DJ, *et al*. Cordycepin inhibits lipopolysaccharide-induced inflammation by the suppression of NF-kappaB through Akt and p38 inhibition in RAW 264.7 macrophage cells. European Journal of Pharmacology. 2006; 545: 192–199. https://doi.org/10.1016/j.ejphar.2006.06.047.

[17] Shin S, Moon S, Park Y, Kwon J, Lee S, Lee CK, *et al*. Role of Cordycepin and Adenosine on the Phenotypic Switch of Macrophages via Induced Anti-inflammatory Cytokines. Immune Network. 2009; 9: 255–264. https://doi.org/10.4110/in.2009.9.6.255.

[18] Shin S, Lee S, Kwon J, Moon S, Lee S, Lee CK, *et al*. Cordycepin Suppresses Expression of Diabetes Regulating Genes by Inhibition of Lipopolysaccharide-induced Inflammation in Macrophages. Immune Network. 2009; 9: 98–105. https://doi.org/10.4110/in.2009.9.3.98.

[19] Liu Z, Lv L, Wei J, Xie Y, Jili M, Huang Y, *et al*. Cordycepin attenuates NLRP3/Caspase-1/GSDMD-mediated LPS-induced

macrophage pyroptosis. Frontiers in Pharmacology. 2025; 16: 1526616. https://doi.org/10.3389/fphar.2025.1526616.

[20] Wei P, Wang K, Luo C, Huang Y, Misilimu D, Wen H, *et al*. Cordycepin confers long-term neuroprotection via inhibiting neutrophil infiltration and neuroinflammation after traumatic brain injury. Journal of Neuroinflammation. 2021; 18: 137. https://doi.org/10.1186/s12974-021-02188-x.

[21] Zhang Y, Cheng J, Su Y, Li M, Wen J, Li S. Cordycepin induces M1/M2 macrophage polarization to attenuate the liver and lung damage and immunodeficiency in immature mice with sepsis via NF-κB/p65 inhibition. The Journal of Pharmacy and Pharmacology. 2022; 74: 227–235. https://doi.org/10.1093/jpp/rgab162.

[22] Basak U, Sarkar T, Mukherjee S, Chakraborty S, Dutta A, Dutta S, *et al*. Tumor-associated macrophages: an effective player of the tumor microenvironment. Frontiers in Immunology. 2023; 14: 1295257. https://doi.org/10.3389/fimmu.2023.1295257.

[23] Zhang W, Wang M, Ji C, Liu X, Gu B, Dong T. Macrophage polarization in the tumor microenvironment: Emerging roles and therapeutic potentials. Biomedicine & Pharmacotherapy. 2024; 177: 116930. https://doi.org/10.1016/j.biopha.2024.116930.

[24] Serpi M, Ferrari V, McGuigan C, Ghazaly E, Pepper C. Synthesis and Characterization of NUC-7738, an Aryloxy Phosphoramidate of 3'-Deoxyadenosine, as a Potential Anticancer Agent. Journal of Medicinal Chemistry. 2022; 65: 15789–15804. https://doi.org/10.1021/acs.jmedchem.2c01348.

[25] Deng Q, Li X, Fang C, Li X, Zhang J, Xi Q, *et al*. Cordycepin enhances anti-tumor immunity in colon cancer by inhibiting phagocytosis immune checkpoint CD47 expression. International Immunopharmacology. 2022; 107: 108695. https://doi.org/10.1016/j.intimp.2022.108695.

[26] McWhorter FY, Wang T, Nguyen P, Chung T, Liu WF. Modulation of macrophage phenotype by cell shape. Proceedings of the National Academy of Sciences of the United States of America. 2013; 110: 17253–17258. https://doi.org/10.1073/pnas.1308887110.

[27] Sridharan R, Cavanagh B, Cameron AR, Kelly DJ, O'Brien FJ. Material stiffness influences the polarization state, function and migration mode of macrophages. Acta Biomaterialia. 2019; 89: 47–59. https://doi.org/10.1016/j.actbio.2019.02.048.

[28] Vogel V, Sheetz M. Local force and geometry sensing regulate cell functions. Nature Reviews. Molecular Cell Biology. 2006; 7: 265–275. https://doi.org/10.1038/nrm1890.